A semi-analytical method to estimate the effective slip length of spreading spherical-cap shaped droplets using Cox theory

M Wörner[1*], X Cai[2,3], H Alla[4] and P Yue[5]

[1] Karlsruhe Institute of Technology (KIT), Institute of Catalysis Research and Technology, Engesserstr. 20, 76131 Karlsruhe, Germany

[2] Karlsruhe Institute of Technology (KIT), Institute for Chemical Technology and Polymer Chemistry, Engesserstr. 20, 76131 Karlsruhe, Germany

[3] Karlsruhe Institute of Technology (KIT), Institute of Fluid Mechanics, Kaiserstr. 10, 76131 Karlsruhe, Germany

[4] Université des Sciences et de la Technologie d'Oran, BP 1505 El M'Naouar Bir el Djir 31000, Oran, Algeria

[5] Virginia Tech, Department of Mathematics, 460 McBryde Hall, Blacksburg, VA 24061-0123, USA

* Corresponding author, E-mail: martin.woerner@kit.edu.

Abstract

The Cox law on dynamic spreading relates the difference between the cubic values of the apparent contact angle (θ) and the equilibrium contact angle to the instantaneous contact line speed (U). Comparing spreading results with this hydrodynamic wetting theory requires accurate data of θ and U during the entire process. We consider the case when gravitational forces are negligible, so that the shape of the spreading drop can be closely approximated by a spherical cap. Using geometrical dependencies, we transform the general Cox law in a semi-analytical relation for the temporal evolution of the spreading radius. Evaluating this relation numerically shows that the spreading curve becomes independent from the gas viscosity when the latter is less than about 1% of the drop viscosity. Since inertia may invalidate the made assumptions in the initial stage of spreading, a quantitative criterion for the time when the spherical-cap assumption is reasonable is derived utilizing phase-field simulations on the spreading of partially wetting droplets. The developed theory allows to compare experimental/computational spreading curves for spherical-cap shaped droplets with Cox theory without the need for instantaneous data of θ and U. Furthermore, the fitting of Cox theory enables estimating the effective slip length. This is potentially useful for establishing relationships between slip length and parameters in numerical methods for moving contact lines.

Keywords: droplet spreading, contact angle, slip length, Cox-Voinov law, phase-field method

1. Introduction

Wetting phenomena such as the spreading of liquids on a solid surface are ubiquitous in nature and technology and of fundamental interest for various scientific disciplines and technical applications (Bonn *et al* 2009). A common approach for describing the dynamic wetting of droplets on solid substrates is relating the macroscopic apparent (dynamic) contact angle (θ), which is the angle to which measurements usually relate, with the static (equilibrium) contact angle (θ_e) and the contact line speed (U). Different forms of this relationship have been proposed by Hoffman (1975), Voinov (1976), Tanner (1979) and Cox (1986). According to the asymptotic hydrodynamic theory of Cox (1986) it is

$$G(\theta,\eta) - G(\theta_e,\eta) = Ca \ln(L / L_S) \tag{1}$$

where

$$G(\theta,\eta) = \int_0^{\theta} \frac{\mathrm{d}\theta}{f_{\mathrm{Cox}}(\theta,\eta)} \tag{2}$$

and

$$f_{\mathrm{Cox}}(\theta,\eta) = \frac{2\sin\theta\left\{\eta^2(\theta^2-\sin^2\theta)+2\eta\left[\theta(\pi-\theta)+\sin^2\theta\right]+\left[(\pi-\theta)^2-\sin^2\theta\right]\right\}}{\eta(\theta^2-\sin^2\theta)\left[(\pi-\theta)+\sin\theta\cos\theta\right]+\left[(\pi-\theta)^2-\sin^2\theta\right](\theta-\sin\theta\cos\theta)} \tag{3}$$

Herein, $\eta := \mu_G / \mu_L$ is the gas-to-drop viscosity ratio. The capillary number $Ca := \mu_L U/\sigma$ represents a non-dimensional contact line speed normalized by the drop viscosity (μ_L) and surface tension (σ). In Eq. (1), L is a characteristic macroscopic (outer) length scale (i.e., the capillary length or the size of a spreading drop) whereas L_S is a microscopic (inner) length scale representing the length of the region where no-slip boundary conditions do not apply. Allowing for slip near the moving contact line overcomes the force singularity appearing for no-slip boundary conditions (Dussan V. and Davis 1974), resulting in finite but large stresses at the contact line (Hocking 1977). These in turn produce rapid changes in curvature since they must be balanced by the capillary pressure and hence a rapid change in slope near the contact line is to be expected (Hocking 1992), an effect often denoted as viscous bending (Blake 2006). However, relaxing the no-slip boundary condition introduces the slip length L_S as new unknown parameter. The value of L_S should be of order of molecular dimensions and the magnitude of the term $\lambda := \ln(L/L_S)$ is expected to be ~10 (Blake 2006). In practice L_S often serves as a *fitting parameter* of the hydrodynamic wetting model (Foister 1990, Eral *et al* 2013). In this paper, we propose a procedure to determine λ by fitting of experimental or numerical results for the time-dependent wetting radius. Relating the fitted value of λ with a suitable macroscopic length scale L yields $L_S = L \exp(-\lambda)$. The corresponding value of L_S can thus be

interpreted as that slip length which best describes the specific droplet spreading process within the hydrodynamic theory of wetting, and is denoted here as "effective" slip length.

The derivation of equations (1) - (3) does not involve any assumption related to the macroscopic shape of the drop. However, for $\theta < 135°$ and very small viscosity ratio ($\eta \to 0$) it is

$$G(\theta,0) - G\left(\theta_e,0\right) \approx (\theta^3 - \theta_e^3)/9 \tag{4}$$

Then, Eq. (1) simplifies to the form

$$\theta^3 = \theta_e^3 + 9Ca \ln\left(\alpha \frac{L}{L_S}\right) \tag{5}$$

The numerical constant α is non-universal and depends on details of the microscopic and macroscopic boundary conditions (Cox 1986, Eggers and Stone 2004, Snoeijer and Andreotti 2013). Eq. (5) is commonly known as the Cox-Voinov law and is valid in the limit $Ca \ll 1$. Since $L \gg L_S$, the dependence of the logarithmic function on L is very weak and thus can be assumed constant. Experiments confirm that the cubic relation $\theta^3 - \theta_e^3 \sim Ca$ holds for contact angles as large as 70 – 100° provided Ca and the Reynolds number $Re := \rho_L LU/\mu_L$ are sufficiently smaller than unity (Fermigier and Jenffer 1991, Wang *et al* 2007).

The principle result in experimental and computational studies on dynamic spreading processes is the time evolution of the radius $a(t)$ of the circular contact area (spreading radius or base radius). Often a comparison of experimental/numerical results with theoretical or empirical relations is of interest, e.g. for model testing or code validation. The comparison with the Cox-Voinov law, Eq. (5), is often performed by displaying $\theta^3 - \theta_e^3$ over Ca (see e.g. Kim *et al* (2015) for a recent experimental study and Pahlavan *et al* (2015) for a recent numerical one). For experiments, this procedure is associated with two disadvantages. First, it requires the measurement or evaluation of $\theta(t)$ during the entire spreading process; this is elaborate and measurements of the apparent contact angle may be ambiguous. Second, it is potentially inaccurate because the contact line speed $U(t) = \mathrm{d}a(t)/\mathrm{d}t$ (spreading speed) is obtained by differentiation, and thus may lead to scattered data.

In this paper, an alternative route is presented for comparing results of dynamic droplet spreading with the Cox or Cox-Voinov laws. We assume that gravitational effects are negligible, which is justified provided a typical pressure variation caused by gravity is much smaller than the Laplace pressure. This precondition is satisfied provided the cubic root of the drop volume is much smaller than the capillary length scale (Elyousfi *et al* 1998). Under these conditions, the spreading is driven by capillary forces alone

and the interface forms at each instant in time a spherical cap. Such a spherical-cap assumption has already been used by several authors (Hocking and Rivers 1982, Foister 1990, McHale *et al* 1994, Seaver and Berg 1994, Rowan *et al* 1995, de Ruijter *et al* 1999, de Ruijter *et al* 2000). Hocking and Rivers (1982) used matched asymptotic expansions to solve the Stokes equation both in the outer region (with spherical cap assumption) and in the vicinity of the contact line and derived a relation for the wetted radius a as function of time (Eq. 6.1), which must be evaluated numerically. Foister (1990) employed the spherical cap assumption to compare experimental spreading data with the hydrodynamic theory. McHale *et al* (1994) utilized it to balance the rate of change of free energy with an approximation for the viscous dissipation in the drop to derive a spreading law for small droplets.

Similar to Hocking and Rivers (1982), we employ in this paper the spherical-cap assumption to derive a semi-analytical relationship for $a(t)$, which must be evaluated numerically as well. In contrast to Hocking and Rivers (1982), we start here from an explicit relation between dynamic contact angle and capillary number, namely Cox law. Using geometrical dependencies following from the spherical-cap assumption, we transform Eq. (1) into a relationship for $a(t)$ which allows easy and straightforward comparisons with experiments and computations. As first novelty of our study, we use this relation to investigate the influence of the gas-liquid viscosity ratio on the spreading of a spherical-cap droplet and show that the spreading curves following Cox theory become independent from the gas viscosity when the viscosity ratio is below about 0.01. While Hocking and Rivers (1982) mention that in experiments the initial drop shape usually deviates notably from a spherical-cap, they also state that it is unclear from which time on the spherical-cap assumption is reasonable. As second novelty of our study, we provide a quantitative criterion for the time when the spherical-cap assumption is reasonable. For this purpose we perform numerical simulations of the spreading of a small droplet on a partially wetting flat substrate using a phase-field method, where we solve the Cahn-Hilliard-Navier-Stokes equations with and without inertia. Finally, we illustrate how comparing the numerical (or experimental) base-radius over time curve with the theoretical one allows extracting an effective slip length. Here, the term *effective* expresses the fact that the slip length in numerical computations is not necessarily equal to the physical slip length, which is on the order of 10^{-9}m or less for most surfaces (Kim *et al* 2015).

2. Theory

In this section, we transform the general Cox law into a time dependent relation for the spreading radius. For this purpose, we consider a drop with constant volume (V) that spreads on a flat chemically

homogenous surface. Our fundamental presupposition is, as mentioned before, that the macroscopic droplet shape is – during the entire spreading process – closely approximated by a spherical cap.

For a sessile drop with spherical cap shape, geometric parameters such as drop height, wetted base radius, spherical cap radius, contact angle and drop volume are linked by unique algebraic relationships (Strella 1970). As a spherical cap has only two degrees of freedom, if a variable is constant it is possible to write all the parameters of the system in function of one variable. For a spherical cap droplet with constant volume V, the spreading radius $a(t)$ and the apparent contact angle $\theta(t)$ are related as (Rowan *et al* 1995, Berthier *et al* 2008)

$$a(t) = \left(\frac{3V}{\pi}\right)^{1/3} f_{\mathrm{geo}}(\theta) \tag{6}$$

where

$$f_{\mathrm{geo}}(\theta) := \frac{\sin\theta}{\left(2 - 3\cos\theta + \cos^3\theta\right)^{1/3}} \tag{7}$$

The time derivative of Eq. (6) is

$$\frac{\mathrm{d}a(t)}{\mathrm{d}t} = \left(\frac{3V}{\pi}\right)^{1/3} f'_{\mathrm{geo}}(\theta)\frac{\mathrm{d}\theta}{\mathrm{d}t} \tag{8}$$

where

$$f'_{\mathrm{geo}}(\theta) = \frac{\mathrm{d}f_{\mathrm{geo}}}{\mathrm{d}\theta} = -\frac{1}{\left(2+\cos\theta\right)\left(2 - 3\cos\theta + \cos^3\theta\right)^{1/3}} \tag{9}$$

With the identity $2 - 3\cos\theta + \cos^3\theta = (1-\cos\theta)^2(2+\cos\theta)$, Eq. (8) takes the form given by Voinov (1976) (Eq. (4.2)) and McHale *et al* (1994).

By introducing $Ca = \mu_{\mathrm{L}}(\mathrm{d}a(t)/\mathrm{d}t)/\sigma$ and $\lambda = \ln(L/L_{\mathrm{S}})$ into Eq. (1), the Cox law can be rewritten in the form

$$\frac{\mathrm{d}a(t)}{\mathrm{d}t} = \frac{\sigma}{\mu_{\mathrm{L}}\lambda}\left[G(\theta,\eta) - G(\theta_{\mathrm{e}},\eta)\right] \tag{10}$$

Combining Eq. (8) and Eq. (10) yields

$$\frac{\sigma}{\mu_{\mathrm{L}}\lambda}\left(\frac{\pi}{3V}\right)^{1/3}\mathrm{d}t = \frac{f'_{\mathrm{geo}}(\theta)}{G(\theta,\eta) - G(\theta_{\mathrm{e}},\eta)}\mathrm{d}\theta \tag{11}$$

An appropriate length scale for transferring Eq. (11) into a non-dimensional form is the volume-equivalent drop radius $R_V := (3V/(4\pi))^{1/3}$. Based on the capillary-viscous time scale $t_{\mathrm{ref}} := \mu_{\mathrm{L}} R_V/\sigma$, the non-dimensional time $\tau := t/t_{\mathrm{ref}} = \sigma t/(\mu_{\mathrm{L}} R_V)$ can be defined. With these definitions Eq. (11) becomes

$$\mathrm{d}\tau = \frac{\sqrt[3]{4}\lambda\, f'_{\mathrm{geo}}(\theta)}{G(\theta,\eta) - G(\theta_{\mathrm{e}},\eta)}\mathrm{d}\theta \tag{12}$$

Eq. (12) constitutes a differential relation between the instantaneous macroscopic contact angle θ and the non-dimensional time τ.

Integrating Eq. (12) requires the specification of initial conditions. Let $\theta_0 \neq \theta_{\mathrm{e}}$ be the initial contact angle at time $t = \tau = 0$. Then, the initial spherical cap radius is

$$R_{\mathrm{S},0} = \left(\frac{3}{\pi}\frac{V}{2-3\cos\theta_0+\cos^3\theta_0}\right)^{1/3} \tag{13}$$

while the initial base radius is $a_0 = R_{\mathrm{S},0}\sin\theta_0$. For $\theta_0 > \theta_{\mathrm{e}}$ the contact line advances as the droplet spreads out and wets the substrate, whereas it recedes for $\theta_0 < \theta_{\mathrm{e}}$ where dewetting occurs.

Integrating Eq. (12) and taking into account Eq. (2) and Eq. (9) yields

$$\tau = -\int_{\theta_0}^{\theta}\left[\int_0^x \frac{\mathrm{d}y}{f_{\mathrm{Cox}}(y,\eta)} - \int_0^{\theta_{\mathrm{e}}} \frac{\mathrm{d}y}{f_{\mathrm{Cox}}(y,\eta)}\right]^{-1} \frac{\sqrt[3]{4}\lambda}{(2+\cos x)(2-3\cos x+\cos^3 x)^{1/3}}\mathrm{d}x \tag{14}$$

In the limit $\eta \to 0$ Eq. (14) simplifies – by virtue of Eq. (4) – to the form

$$\tau = -\int_{\theta_0}^{\theta} \frac{9}{x^3-\theta_{\mathrm{e}}^3}\frac{\sqrt[3]{4}\lambda}{(2+\cos x)(2-3\cos x+\cos^3 x)^{1/3}}\mathrm{d}x \tag{15}$$

The integrals on the right-hand-sides of Eq. (14) and (15) cannot be solved analytically. However, for a given value of θ either integral can be solved numerically. Doing this for a set of distinct values θ_i in the range $\theta_{\mathrm{e}} < \theta_i < \theta_0$ (spreading case) yields the corresponding set of discrete values of non-dimensional time τ_i. From the discrete values θ_i, one obtains from Eq. (6) the corresponding discrete values of the spreading radius a_i, and from the discrete values of τ_i the discrete values of t_i. Thus, a relation between a_i and t_i is established which can be used to compare the spreading dynamics of Cox theory with computational or experimental results.

Due to the lack of analytical solutions for the integrals in Eq. (14) and Eq. (15), each combination of θ_{e}, θ_0 and η requires a separate numerical integration. This numerical solution applies by virtue of the non-

dimensional time to different liquid properties and initial drop volumes. To perform the numerical integration, a MATLAB script is used (see supplemental material) where the discrete values of the contact angle are given by $\theta_i = \theta_0 - i \cdot \delta\theta$ for $i = 1,2,3,\ldots$. Here, the step size $\delta\theta = 0.001$ is used. The procedure for dewetting ($\theta_0 < \theta_e$) is similar and the MATLAB script can easily be adapted to handle this case as well.

3. Numerical simulation

In this section, the governing equations and numerical set-up for simulating the spreading of a liquid droplet on a perfectly smooth, chemically homogenous, solid surface are presented. The simulations are performed with a phase-field method as implemented in an in-house finite element code denoted as AMPHI (Yue *et al* 2006, Yue *et al* 2010).

3.1 Phase-field method

In the phase-field method (Jacqmin 1999, Villanueva and Amberg 2006, Ding *et al* 2007, Khatavkar *et al* 2007, He and Kasagi 2008, Kim 2012), the order parameter ϕ serves to describe the distribution of the gas and liquid phases. Here, ϕ takes distinct values $\phi_L = 1$ and $\phi_G = -1$ in the bulk phases and varies rapidly but smoothly in a thin transition layer (the diffuse interface). The location of the gas-liquid interface is represented by $\phi = 0$. To determine the phase evolution, the convective Cahn-Hilliard (CH) equation

$$\frac{\partial \phi}{\partial t} + \mathbf{u} \cdot \nabla \phi = M \nabla^2 J_B \tag{16}$$

is solved, where

$$J_B(\phi) = \frac{3}{2\sqrt{2}} \frac{\sigma}{\varepsilon} \left[\phi(\phi^2 - 1) - \varepsilon^2 \nabla^2 \phi \right] \tag{17}$$

is the bulk chemical potential. In the latter equations, M is the (constant) mobility parameter and ε is a positive constant determining the interfacial thickness. The Cahn number $Cn := \varepsilon / R_V$ relates the interfacial width parameter to the volume-equivalent drop radius.

In this paper, we consider two incompressible, immiscible, isothermal Newtonian fluids with constant physical properties. The flow of both phases is described by the single-field Navier-Stokes equations

$$\nabla \cdot \mathbf{u} = 0 \tag{18}$$

$$\rho \left(\frac{\partial \mathbf{u}}{\partial t} + \mathbf{u} \cdot \nabla \mathbf{u} \right) = -\nabla p + \nabla \cdot \mu \left[\nabla \mathbf{u} + (\nabla \mathbf{u})^T \right] + \rho \mathbf{g} + \mathbf{f}_{st} \tag{19}$$

The density field and the viscosity field depend on the phase distribution and are computed as

$$\rho(\mathbf{x},t) = \rho_{\mathrm{G}}(1-H_{\phi}) + \rho_{\mathrm{L}}H_{\phi}, \qquad \mu(\mathbf{x},t) = \mu_{\mathrm{G}}(1-H_{\phi}) + \mu_{\mathrm{L}}H_{\phi} \tag{20}$$

Here, $H_{\phi} = (1 + \phi) / 2$ is a regularized Heaviside function computed from the order parameter. The last term in Eq. (19) represents the surface tension force which is expressed in AMPHI as $\mathbf{f}_{\mathrm{st}} = J_{\mathrm{B}}\nabla\phi$.

Within the wall energy relaxation model (Yue and Feng 2011), the following boundary conditions apply on the solid substrate:

$$\mathbf{u} = \mathbf{u}_{\mathrm{w}} \tag{21}$$

$$\mathbf{n}_{\mathrm{w}} \cdot \nabla J_{\mathrm{S}} = 0 \tag{22}$$

$$\frac{\partial\phi}{\partial t} + \mathbf{u}_{\mathrm{w}} \cdot \nabla\phi = -\Gamma J_{\mathrm{S}} \tag{23}$$

Here, $\mathbf{u}_{\mathrm{w}}$ is the wall velocity (which is set to zero here), Γ is a rate constant and

$$J_{\mathrm{S}} = \frac{3\sigma}{4}\left[\sqrt{2}\varepsilon\mathbf{n}_{\mathrm{w}} \cdot \nabla\phi - (1-\phi^2)\cos\theta_{\mathrm{e}}\right] \tag{24}$$

is the surface chemical potential. For the present simulations, we adopt the energy equilibrium model (limit $\Gamma \to \infty$) where the latter two equations can be combined to yield

$$\mathbf{n}_{\mathrm{w}} \cdot \nabla\phi = \frac{\cos\theta_{\mathrm{e}}}{\sqrt{2}\varepsilon}(1-\phi^2) \tag{25}$$

This boundary condition is consistent with the Cox theory in the sense that the interface retains the equilibrium contact angle within the slip zone ($z \le L_{\mathrm{S}}$), whereas the apparent contact angle in the outer zone is the result of viscous force bending the interface ($z >> L_{\mathrm{S}}$). The same two-region picture can be borrowed into the CH solution, except that the length scale of the inner region, the diffusion length L_{D} (cf. Section 4.4), will be artificially enlarged. Furthermore, wall energy relaxation – when considered – competes with CH diffusion in defining the apparent contact angle, the former tending to "rotate" the interface at the contact line while the latter to "bend" it in the bulk (Yue and Feng 2011).

While the wetting boundary condition given by Eq. (25) is often used in phase field simulations, it is valid only under the tacit assumption of a perfectly smooth chemically homogenous substrate. In reality, dynamic spreading processes are usually affected by topographical or chemical surface heterogeneities. To account for these heterogeneities, upscaled/homogenized Cahn-Hilliard phase-field methods have been proposed (Wylock *et al* 2012, Schmuck *et al* 2012) but are mainly applied for flow through porous media so far (Ververis and Schmuck 2017).

3.2 Computational set-up and fluid properties

Figure 1 shows the polar coordinate systems and a sketch of the initial and equilibrium droplet shapes. The initial shape is a hemisphere so that the initial contact angle is $\theta_0 = 90°$. The initial spherical cap radius is $R_{S,0} = a_0 = 0.5$ mm. This corresponds to a drop volume $V = 0.2618$ mm^3 and volume-equivalent drop radius $R_V = 0.397$ mm. The equilibrium contact angle is set to $\theta_e = 60°$. Thus, the ratio between terminal and initial spreading radius is

$$\frac{a_e}{a_0} = \left(\frac{2 - 3\cos\theta_0 + \cos^3\theta_0}{2 - 3\cos\theta_e + \cos^3\theta_e} \right)^{1/3} \sin\theta_e = \sqrt[3]{\frac{2}{5}}\sqrt{3} = 1.276 \tag{26}$$

The liquid phase is coconut oil with a density $\rho_L = 910$ kg/m^3 and dynamic viscosity $\mu_L = 0.03$ Pa s. The gas density is $\rho_G = 1$ kg/m^3 and the coefficient of surface tension is $\sigma = 0.0294$ N/m. The gas viscosity is $\mu_G = 3\times10^{-4}$ Pa·s corresponding to $\eta = 0.01$. The value of the capillary-viscous time scale is $t_{ref} = 0.405$ ms. The already mentioned criterion of Elyousfi et al. (1998) for neglecting gravity reads $V^{1/3} = (4\pi R_V^3/3)^{1/3} \ll (\sigma / g(\rho_L - \rho_G))^{0.5}$. This condition is equivalent to $Eo \ll 0.77$, where $Eo := (\rho_L - \rho_G) g R_V^2 / \sigma$ is the Eötvös number. In the present simulation it is $Eo = 0.0487$ so that gravitational effects are negligible. In the simulations, gravity is therefore neglected ($g = 0$) so that the spreading is driven by capillarity alone.

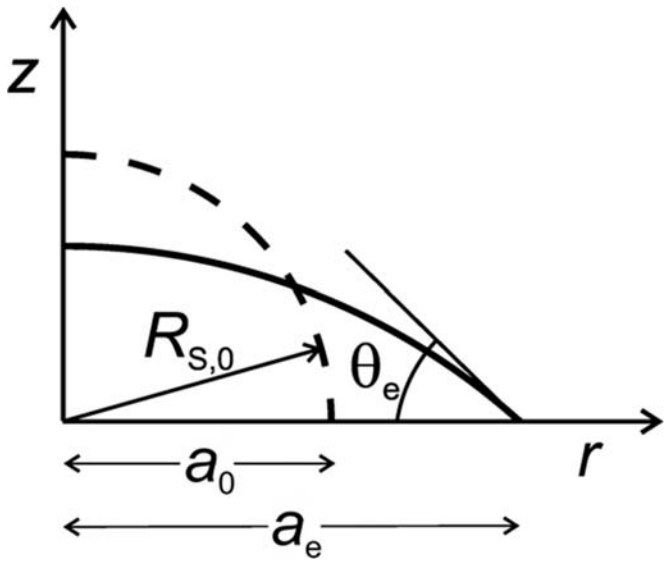

Figure 1. Schematic illustration of the polar coordinate system with initial drop shape (dashed line, contact angle $\theta_0 = 90°$) and final drop shape (solid line, equilibrium contact angle $\theta_e < \theta_0$).

The 2D computational domain is a square with size $0 \le r \le H$ and $0 \le z \le H$. In order to minimize the influence of the domain size $H = 3R_{S,0}$ is used. The boundary conditions are as follows. At the axis ($r = 0$) axi-symmetry is specified. At the top and right boundaries of the computational domain ($r = z = H$) constant pressure inlet boundary conditions are applied. At the flat and smooth solid surface ($z = 0$) the no-slip condition holds. The boundary condition for the order parameter at the solid surface, Eq. (25), employs the equilibrium contact angle ($\theta_e = 60°$), independent from the contact line speed. Thus at the present stage, neither a dynamic contact angle model is used nor is contact angle hysteresis taken into account. In the phase field method, the apparent contact angle determined at a certain distance away from the wall may nevertheless differ from θ_e as discussed above, see also Yue and Feng (2011) and Kusumaatmaja *et al* (2016).

4. Results and discussion

In this section, we discuss some implications and limitations of the theoretical derivation presented above and compare numerical results for the time evolution of the spreading radius with the corresponding curve derived from Cox theory using the MATLAB script.

4.1 Influence of viscosity ratio

We first discuss the influence of the viscosity ratio (η) on the motion of the contact line for the general Cox law. Since Eq. (14) is linear with respect to $\lambda = \ln (L/L_S)$, it is sufficient to consider one value only (here $\lambda = 10$). Figure 2 shows the time evolution of the spreading radius (normalized by the initial value a_0) for four different values of η, namely 0, 0.01, 0.1 and 1. It is obvious that the spreading curves for $\eta = 0$ and $\eta = 0.01$ are almost identical. This indicates that the influence of the gas viscosity on the spreading process is negligible for $\eta \le 0.01$. As η increases, the spreading process is delayed. We remark that the curve for $\eta = 1$ in Figure 2 is not consistent with the Cox-Voinov law, Eq. (5), since the underlying approximation in Eq. (4) is only valid in the limit of very small viscosity ratio.

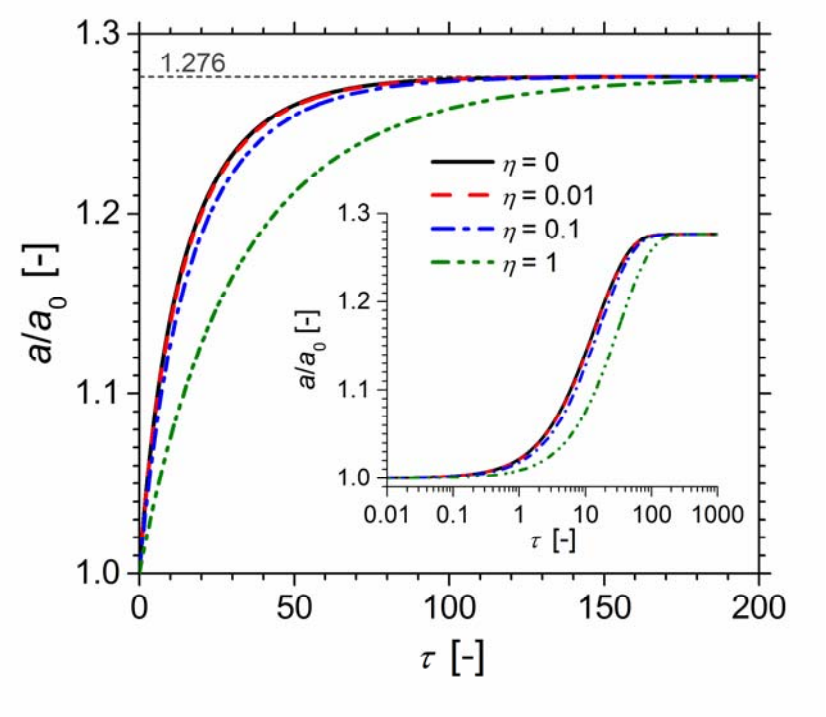

Figure 2. Influence of gas-liquid viscosity ratio (η) on the spreading of a spherical-cap droplet following the Cox theory for $\lambda = 10$.

4.2 Limitations for initial stage of spreading

Even when gravitational forces are negligible, the above theory may become invalid for comparison with experimental or computational results in the initial stage of spreading for two reasons. First, the theory in Section 2 relies on the assumption that at each instant in time of the spreading process the drop forms a spherical cap. Due to the boundary conditions for the contact angle given by Eq. (25), the contact angle in the present phase-field simulation immediately adapts from the initial value θ_0 to the equilibrium value θ_e, see Figure 3 a), while away from the wall the interface remains at its initial shape. Thus, at least in the very first stage of the simulation, the drop shape differs from a spherical cap and invalidates a comparison of the computational results with the above theory.

The mentioned distortion of the interface near the contact line can induce a capillary wave that travels up the drop and may even result in drop ejection (Ding *et al* 2012). In this context, it is useful to perform a simple estimation of the time t_{cw} when the capillary wave is diminished so that for larger times an agreement between the numerical results and Cox theory may be expected. The speed of a capillary wave with wave length Λ is $U_{cw} \sim \sqrt{2\pi\sigma / (\Lambda\rho_L)}$. The time required for this wave to travel a distance L_{cw} is

$$t_{\mathrm{cw}} = \frac{L_{\mathrm{cw}}}{U_{\mathrm{cw}}} \sim \sqrt{\frac{\rho_L \Lambda L_{\mathrm{cw}}^2}{2\pi\sigma}} \tag{27}$$

For evaluation of t_{cw} we assume that the capillary wave travels from the contact line to the drop apex and back so that $L_{\mathrm{cw}} = \pi R_0$. As a rough approximation for the mean wave length of the capillary wave during this period we take one half of the distance from the contact line to the drop apex so that $\Lambda = \pi R_0 / 4$. Then Eq. (27) yields $t_{\mathrm{cw}} \sim \sqrt{\pi^2 \rho_L R_0^3 / (8\sigma)} = 2.2\,\mathrm{ms}$ corresponding to $\tau_{\mathrm{cw}} \sim 5.4$.

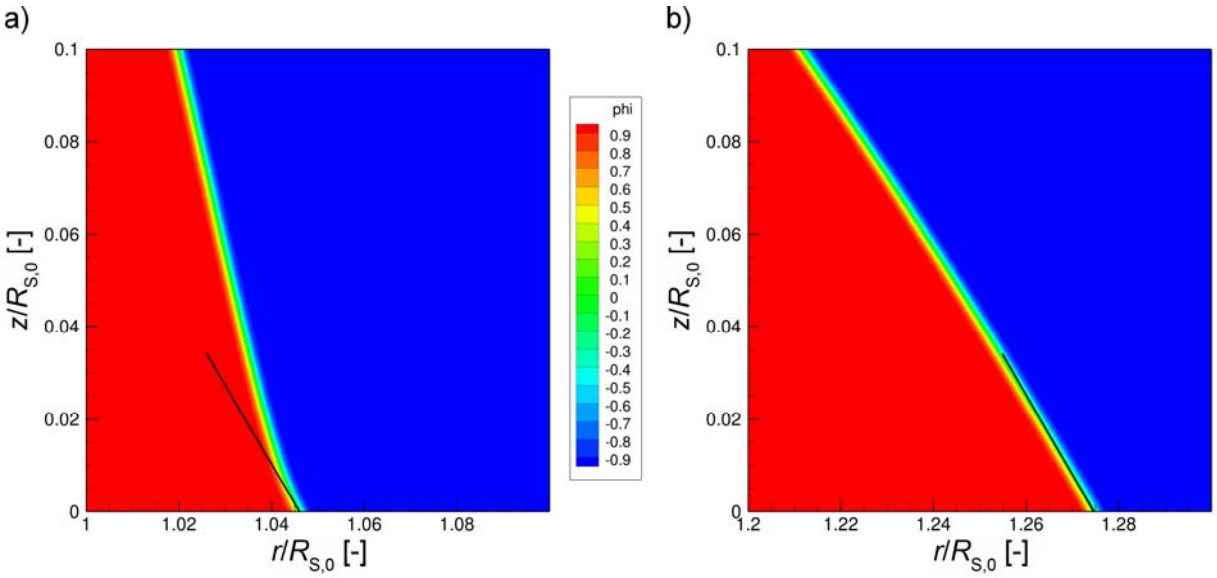

Figure 3. Zoom of the computed order parameter field near the contact line for two instants in time (simulation with inertia). a) Initial stage of spreading ($\tau = 0.987$), b) final equilibrium state ($\tau = 116.4$). The slope of the straight black line in each subfigure corresponds to the equilibrium contact angle $\theta_e = 60°$.

Another possible reason why a good agreement between the simulation results and Cox theory may not be expected for short times is inertia, as the simulations start from a static state where the droplet is at rest. The non-dimensional spreading curves $a(\tau)/a_0$ displayed in Figure 2 arise from pure kinematic relations not accounting for inertia. The time-derivative of these curves yields the contact line velocity

$$U(\tau) = \frac{\mathrm{d}a}{\mathrm{d}t} = \frac{\sigma}{\mu_{\mathrm{L}}} \frac{a_0}{R_{\mathrm{V}}} \frac{\mathrm{d}}{\mathrm{d}\tau} \left(\frac{a(\tau)}{a_0} \right) \tag{28}$$

so that the time evolutions of the capillary number

$$Ca(\tau) = \frac{\mu_L U(\tau)}{\sigma} = \frac{a_0}{R_V} \frac{\mathrm{d}}{\mathrm{d}\tau}\left(\frac{a(\tau)}{a_0} \right) \tag{29}$$

and the Reynolds number

$$Re(\tau) = \frac{\rho_L R_V U(\tau)}{\mu_L} = \frac{Ca(\tau)}{Oh^2} \tag{30}$$

can be computed. Here, $Oh := \mu_L / (\rho_L \sigma R_V)^{0.5}$ denotes the Ohnesorge number. The maximum values of $Ca(\tau)$ and $Re(\tau)$ are obtained for the limit $\tau \to +0$. While the maximum value of the capillary number may be less than unity, the maximum value of the Reynolds number may be larger than unity when the Ohnesorge number is low. Thus, the requirement $Re < 1$ for the Cox-Voinov theory to be valid may be not met in the initial stage of the computations. In the present numerical study, the Ohnesorge number $Oh = 0.291$ is smaller than unity, which indicates that inertia may have an influence in the initial stage of spreading. The theory for spherical-cap droplets in Section 2 does not consider the effect of inertia. For small values of τ, the numerical spreading curves may thus be delayed as compared to those computed from Cox theory.

4.3 Effect of inertia

To quantify the effect of inertia, two phase-field simulations are performed for the same value of $Oh = 0.291$; once with and once without inertia. The computations are carried out with the AMPHI code that employs Galerkin finite elements on an adaptive triangular grid that adequately resolves the interfacial region. In this test case, $\varepsilon = 0.5$ µm corresponding to $\varepsilon / R_{S,0} = 0.001$ and $Cn = 0.00126$ is used. The mobility is $M = 8.33 \cdot 10^{-11}$ m^{3}s/kg while the gas-liquid viscosity ratio is set to $\eta = 0.01$. According to Figure 2, the results for $\eta = 0.01$ should not differ from those for $\eta = 0.0005$ corresponding to the dynamic viscosity of air ($\mu_G = 1.5 \cdot 10^{-5}$ Pa s). With these parameters the diffuse interface is very thin but at the same time very well resolved by the adaptive finite element mesh. Consequently, the simulations fulfil the criteria for the sharp-interface limit of the phase-field method (Yue *et al* 2010).

Figure 4 shows the time evolution of the spreading radius (normalized by the initial value a_0) computed by AMPHI with and without inertia. Included in this figure are for comparison two semi-analytical curves of the Cox law where the phenomenological parameter $\lambda = \ln (L/L_S)$ is set to 5 and 6, respectively. For both numerical simulations with and without inertia, the terminal spreading radius agrees well with the analytical value. The influence of inertia on the spreading process is rather small but still notable, which is consistent with the value of Oh. As expected, inertia tends to slow down the spreading process in the initial stage but speeds it up in the final stage. Figure 3 b) shows the terminal field of the order parameter in the simulation

with inertia in the vicinity of the contact line. The slope of the interface corresponds well with the equilibrium contact angle while the value of the terminal spreading radius agrees well with the analytical value given in Eq. (26).

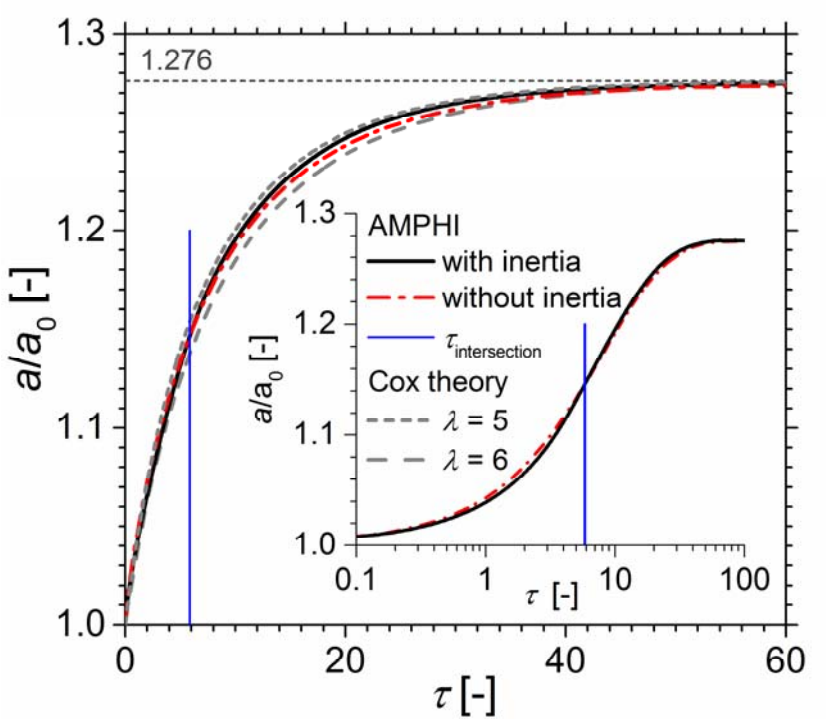

Figure 4. Time evolution of normalized spreading radius $a(\tau)/a0$. Comparison of simulations results with and without inertia force with Cox theory.

Biance *et al* (2004) estimated the duration of the inertial regime as

$$t_{\text{inertial}} \sim \left(\frac{\rho_{\text{L}} \sigma R_V}{\mu_{\text{L}}^2} \right)^{1/8} \sqrt{\frac{\rho_{\text{L}} R_V^3}{\sigma}} \tag{31}$$

Though this relation was developed for completely wetting liquids, it may be useful for the present case of partially wetting liquids as well. When normalizing Eq. (31) by the capillary-viscous time scale, it follows

$$\tau_{\text{inertial}} := \frac{t_{\text{inertial}}}{t_{\text{ref}}} = K \cdot Oh^{-5/4} \tag{32}$$

where K is an (unknown) non-dimensional pre-factor. In the present case it is $Oh^{-5/4} = 4.676$. To determine K, we utilize the spreading curves with and without inertia displayed in Figure 4. Both curves intersect at $\tau = 5.86$ as indicated by the vertical line. Assuming that this intersection-time is representative for τ_{inertial} allows to determine the pre-factor in Eq. (32). Here, it follows $K = 1.253$. For the present case, the values of τ_{inertial} and τ_{cw} are thus very similar.

The value of the normalized spreading radius at the inertial cross-over time is $a(\tau_{\mathrm{inertial}})/a_0 = 1.1465$. The corresponding instantaneous contact angle $\theta_{\mathrm{inertial}}$ can be determined by solving Eq. (6) iteratively. Here, one obtains $\theta_{\mathrm{inertial}} = 73.51°$. The instantaneous values of the capillary number and Reynolds number are $Ca(\tau_{\mathrm{inertial}}) = 0.02$ and $Re(\tau_{\mathrm{inertial}}) = 0.24$, respectively. Running the MATLAB script with the initial contact angle $\theta_{\mathrm{inertial}} = 73.51°$ for different values of λ, yields a family of spreading curves beginning at τ_{inertial}. Figure 5 shows the corresponding spreading curves for $\lambda = 5$ and $\lambda = 6$ (with the vertical line denoting $\tau_{\mathrm{inertial}} = 5.86$). The curve for $\lambda = 5$ almost overlaps with the numerical spreading curve (case with inertia). When an appropriate value for the macroscopic length scale L is specified, this result can be used to estimate the effective slip length in the simulation. For example, following Chebbi (2010) and setting $L = R_V = 0.397$ mm yields $L_S \approx R_V \cdot \exp(-5) \approx 2.67$ μm. Often, L is also associated with the capillary length (Snoeijer and Andreotti 2013). Setting $L = (\sigma/(g\Delta\rho))^{0.5} = 1.8$ mm then gives the larger value $L_S \approx 12.1$ μm.

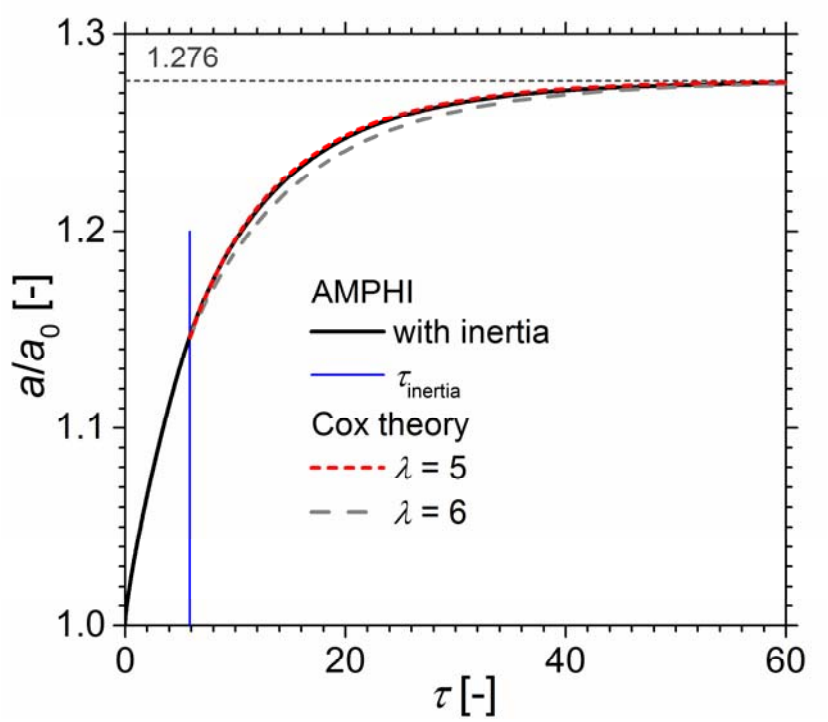

Figure 5. Time evolution of normalized spreading radius $a(\tau)/a0$. Comparison of simulation result with inertia with Cox theory computed with $\theta_0 = \theta_{inertial} = 73.51°$.

4.4 Relation between slip length and diffusion length in phase-field method

In the phase-field method, there exists in addition to ε (which represents the length scale over which ϕ varies) a much larger length scale L_D over which the Cahn-Hilliard diffusion takes place (and over which the chemical potential and the velocity vary). Since diffusion is the driving mechanism for contact line motion in the phase-field method, the slip length L_S is closely related to L_D. Yue and Feng (2011) performed phase field simulations of droplet spreading on a partially wetting substrate using the wall energy relaxation model. They considered the case of matched viscosities ($\eta = 1$) and showed that a universal spreading curve agreeing with Cox theory can be achieved by a certain compensation strategy between the relaxation parameter and Cahn-Hilliard bulk diffusion. More recently, Kusumaatmaja *et al* (2016) performed extensive phase-field simulations for a plug in planar Couette and Poiseuille flow to determine the slip length under the restrictions of Stokes flow, matched phase viscosities ($\mu_L = \mu_G = \mu$) and neutral equilibrium contact angle ($\theta_e = 90°$). The authors identified two regimes with different scaling, depending whether the ratio L_D / ε with $L_D = (M \mu)^{0.5}$ is larger (sharp interface limit) or smaller (diffuse

interface limit) than unity. Furthermore, the dependence of the apparent contact angle on the capillary number was found to be in excellent agreement with Cox theory.

For non-matched viscosity ratios, Yue *et al* (2010) proposed the relation $L_D = (M\ \mu_{eff})^{0.5}$ where $\mu_{eff} = (\mu_L \mu_G)^{0.5} = \mu_L \eta^{0.5}$ is an effective viscosity. The authors also introduced the non-dimensional group

$$S := \frac{L_D}{L} = \frac{(M \mu_L)^{0.5} \eta^{0.25}}{L} \tag{33}$$

Similar to Jacqmin (2000), Yue *et al* (2010) suggested a linear relationship between slip length and diffusion length. Introducing $L_S = \beta L_D$ into $\lambda = \ln (L/L_S)$ then yields

$$\beta = S^{-1} \exp(-\lambda) = \frac{\exp(-\lambda)}{\eta^{0.25}} \frac{L}{(M \mu_L)^{0.5}} \tag{34}$$

Fitting the spreading curve of a phase-field simulation performed with given parameters μ_L, η and M by a certain value of λ thus allows determining β from Eq. (34). For the simulation with AMPHI, Figure 5 suggests $\lambda \approx 5$. Evaluating Eq. (34) for $L = R_V$ yields $\beta \approx 5.3$, a value which is about twice as large as in the relation $\lambda_S = 2.5\lambda_D$ suggested by Yue *et al* (2010). The largest uncertainty here, arises probably from the relationship $\mu_{eff} = (\mu_L \mu_G)^{0.5} = \mu_L \eta^{0.5}$ which has been proposed in an ad hoc manner without deeper scientific foundation.

The semi-analytical procedure developed in this paper may be of particular benefit for the advancement of numerical methods for moving contact lines. For the phase-field method, it offers the opportunity to refine Eq. (34) and establish a clear quantitative relationship between the mobility and the effective slip length L_S for droplet spreading phenomena with non-matched viscosities. Similar to the scaling found by Kusumaatmaja *et al* (2016) for a meniscus displacing with constant speed, this relation should be unique and independent of discretization and code implementation; at least as long as the diffuse interface is well resolved. The only uncertainty is the effective viscosity. Establishing such a relation for the phase-field method requires – especially for cases where the contact line speed is not constant in time – considerable computations for a wide parameter space. This is beyond the scope of this paper but will be considered in future work.

For sharp interface methods there is no such relation as Eq. (34). From literature it is known that flows involving moving contact lines computed by the volume-of-fluid (VOF) method are often mesh dependent (Renardy *et al* 2001, Schönfeld and Hardt 2009, Afkhami *et al* 2009, Legendre and Maglio 2015). As a remedy, Renardy *et al* (2001) related the slip length in their VOF method to the grid resolution near the wall

while Afkhami *et al* (2009) proposed a mesh-dependent dynamic contact angle model. The procedure developed in the present paper may be used to establish quantitative relationships between effective slip length and grid resolution for sharp interface methods as well. For convenience, we shortly summarize this procedure in the next subsection.

4.5 Procedure for estimating the effective slip length from spreading curves

In this paper, a semi-analytical procedure is presented that allows estimating the effective slip length L_S of spreading droplets from base-radius over time curves obtained either from numerical computations or from experiments. The procedure is meaningful if two preconditions are met. First, the maximum values of the capillary number and the Reynolds number must both be sufficiently smaller than unity. Second, the spherical-cap assumption must be justified. The latter condition is directly linked to the influence of gravitational forces and is easily met in numerical computations where gravity is set to zero. In computations with gravity and in experiments, gravitational effects are negligible provided the Eötvös number is sufficiently small. Results of numerical studies (Chen *et al* 2009, Dupont *et al* 2011, Cai *et al* 2015) indicate that for the terminal drop shape this is the case for $Eo \leq 0.1$.

When the above preconditions are met, the procedure consists of the following four steps:

1. Compute the Ohnesorge number $Oh = \mu_L / (\rho_L \sigma R_V)^{0.5}$ and estimate from Eq. (32) the duration of the inertial regime $\tau_{inertial} = K \cdot Oh^{-5/4}$ by using either the present value of the pre-factor ($K = 1.253$) or simply $K = 1$.
2. Determine from the instantaneous (numerical or experimental) value of the spreading radius at the inertial time $a(\tau_{inertial})$ the corresponding instantaneous contact angle $\theta_{inertial}$ by solving Eq. (6) iteratively.
3. Run the present MATLAB script (see supplemental material) with $\theta_0 = \theta_{inertial}$ to determine the spreading curves of the general Cox law for different values of $\lambda = \ln (L/L_S)$.
4. Determine the value $\lambda = \lambda_{fit}$ which best fits to the experimental or numerical spreading curve for $\tau \geq \tau_{inertial}$ and estimate the effective slip length by relation $L_S \approx L \exp(-\lambda_{fit})$ with an appropriate value of the macroscopic length scale (L), e.g. $L = R_V$ as used here.

5. Conclusions

Experimental or computational results on spreading processes naturally emerge as base-radius over time curves. In this paper, a semi-analytical method is presented that allows direct comparison of such curves with those arising from the general Cox relation between apparent contact angle and contact line speed. The approach is valid when the capillary number and Reynolds number are both sufficiently smaller than unity and when gravitational effects are negligible so that the drop forms at each instant in time a spherical cap. For these conditions it is shown that the spreading dynamics according to the general Cox law become independent from the gas viscosity when the gas-liquid viscosity ratio is below about 0.01.

The presented procedure is useful for a straightforward comparison of computational or experimental results on droplet spreading in the capillary-viscous regime with Cox theory. To exclude the effect of inertia, which may invalidate the comparison with Cox theory for the initial stage of spreading, a non-dimensional time scale (τ_{inertial}) is derived when the effect of inertia has diminished. This time scale is related to the Ohnesorge number by a power law. For times larger than τ_{inertial}, comparison of computational or experimental spreading curves with Cox theory allows fitting of $\lambda = \ln(L/L_S)$ and thus determining the effective slip length.

A potential advantage of the presented semi-analytical method for experimental studies is that for comparison with Cox theory neither a measurement of the apparent contact angle nor a computation of the contact line speed by differentiation of the spreading radius is necessary. However, the preconditions for validity of the method (especially the spherical-cap assumption) may be quite restrictive and require a sensitive experimental system and careful selection of the solid/liquid pair.

For numerical computations, the spherical-cap assumption is not as restrictive as in experiments since the gravity force can be turned off so that the spreading is driven by capillary forces alone. The semi-analytical procedure developed in this paper may thus be in particular useful for the advancement of numerical methods for moving contact lines. For phase-field methods, it offers the opportunity to establish a quantitative relationship between the effective slip length and the mobility (which is usually treated as a numerical parameter rather than a physical one) for the practically relevant case of droplet-spreading with non-matched viscosities. In order to establish such a relationship, considerable computations for a wide parameter space are required. This task will be considered in future work.

For spreading processes where gravitational forces are not negligible, the drop shape will deviate from a spherical cap. Similar as noted by Hocking and Rivers (1982) for their analytical study, the present method may be extended to such situations by introducing an appropriate (yet unknown) functional relationship for the instantaneous drop shape (e.g. in terms of the Eötvös number) into Eq. (6).

Acknowledgements

M.W. and X.C. acknowledge the financial support by Helmholtz Energy Alliance "Energy-efficient chemical multiphase processes" (HA-E-0004). X.C. is grateful for the Research Travel Grant funded by the Karlsruhe House of Young Scientists (KHYS) to support his research stay at Virginia Tech. P.Y. acknowledges the support by NSF-DMS (Grant No. 1522604). The authors also acknowledge fruitful discussions with M. Ben Said (M.W., X.C., H.A.) and useful suggestions concerning the manuscript by M. Marengo (H.A.).

Supplementary material

A MATLAB script is provided that performs the numerical integration of Eq. (14) for a set of discrete contact angles. This yields the discrete time evolution of the spreading radius according to Cox theory (for which a sample output is provided as well). This material is available free of charge via the Internet.

References

Afkhami S, Zaleski S and Bussmann M 2009 A mesh-dependent model for applying dynamic contact angles to VOF simulations *J. Comput. Phys.* **228** 5370-89

Berthier E, Warrick J, Yu H and Beebe D J 2008 Managing evaporation for more robust microscale assays Part 1. Volume loss in high throughput assays *Lab on a Chip* **8** 852-9

Biance A L, Clanet C and Quere D 2004 First steps in the spreading of a liquid droplet *Physical Review E* **69**

Blake T D 2006 The physics of moving wetting lines *J. Colloid Interface Sci.* **299** 1-13

Bonn D, Eggers J, Indekeu J, Meunier J and Rolley E 2009 Wetting and spreading *Rev. Mod. Phys.* **81** 739-805

Cai X, Marschall H, Wörner M and Deutschmann O 2015 Numerical Simulation of Wetting Phenomena with a Phase-Field Method Using OpenFOAM® *Chem. Eng. Technol.* **38** 1985-92

Chebbi R 2010 A Model for the Dynamics of Partial Wetting *J Chem Eng Jpn* **43** 333-41

Chen Y M, Mertz R and Kulenovic R 2009 Numerical simulation of bubble formation on orifice plates with a moving contact line *Int. J. Multiphase Flow* **35** 66-77

Cox R G 1986 The Dynamics of the Spreading of Liquids on a Solid-Surface. Part 1. Viscous-Flow *J. Fluid Mech.* **168** 169-94

de Ruijter M J, Charlot M, Voue M and De Coninck J 2000 Experimental evidence of several time scales in drop spreading *Langmuir* **16** 2363-8

de Ruijter M J, De Coninck J and Oshanin G 1999 Droplet spreading: Partial wetting regime revisited *Langmuir* **15** 2209-16

Ding H, Li E Q, Zhang F H, Sui Y, Spelt P D M and Thoroddsen S T 2012 Propagation of capillary waves and ejection of small droplets in rapid droplet spreading *J. Fluid Mech.* **697** 92-114

Ding H, Spelt P D M and Shu C 2007 Diffuse interface model for incompressible two-phase flows with large density ratios *J. Comput. Phys.* **226** 2078-95
Dupont J B, Legendre D and Morgante A M 2011 Numerical Simulation for Two-Phase Flows in Fuel Cell Minichannels *J Fuel Cell Sci Tech* **8** 041008-1 - -7
Dussan V. E B and Davis S H 1974 On the Motion of a Fluid-Fluid Interface Along a Solid-Surface *J. Fluid Mech.* **65** 71-95
Eggers J and Stone H A 2004 Characteristic lengths at moving contact lines for a perfectly wetting fluid: the influence of speed on the dynamic contact angle *J. Fluid Mech.* **505** 309-21
Elyousfi A B A, Chesters A K, Cazabat A M and Villette S 1998 Approximate solution for the spreading of a droplet on a smooth solid surface *J. Colloid Interface Sci.* **207** 30-40
Eral H B, 't Mannetje D J C M and Oh J M 2013 Contact angle hysteresis: a review of fundamentals and applications *Colloid Polym Sci* **291** 247-60
Fermigier M and Jenffer P 1991 An Experimental Investigation of the Dynamic Contact-Angle in Liquid Liquid-Systems *J. Colloid Interface Sci.* **146** 226-41
Foister R T 1990 The Kinetics of Displacement Wetting in Liquid Liquid Solid Systems *J. Colloid Interface Sci.* **136** 266-82
He Q W and Kasagi N 2008 Phase-Field simulation of small capillary-number two-phase flow in a microtube *Fluid Dyn. Res.* **40** 497-509
Hocking L M 1977 Moving Fluid Interface. Part 2. Removal of Force Singularity by a Slip-Flow *J. Fluid Mech.* **79** 209-29
Hocking L M 1992 Rival Contact-Angle Models and the Spreading of Drops *J. Fluid Mech.* **239** 671-81
Hocking L M and Rivers A D 1982 The Spreading of a Drop by Capillary Action *J. Fluid Mech.* **121** 425-42
Hoffman R L 1975 Study of Advancing Interface .1. Interface Shape in Liquid-Gas Systems *J. Colloid Interface Sci.* **50** 228-41
Jacqmin D 1999 Calculation of Two-Phase Navier-Stokes Flows Using Phase-Field Modeling *J. Comput. Phys.* **155** 96-127
Jacqmin D 2000 Contact-line dynamics of a diffuse fluid interface *J. Fluid Mech.* **402** 57-88
Khatavkar V V, Anderson P D and Meijer H E H 2007 Capillary spreading of a droplet in the partially wetting regime using a diffuse-interface model *J. Fluid Mech.* **572** 367-87
Kim J 2012 Phase-Field Models for Multi-Component Fluid Flows *Commun Comput Phys* **12** 613-61
Kim J H, Kavehpour H P and Rothstein J P 2015 Dynamic contact angle measurements on superhydrophobic surfaces *Phys. Fluids* **27**
Kusumaatmaja H, Hemingway E J and Fielding S M 2016 Moving contact line dynamics: from diffuse to sharp interfaces *J. Fluid Mech.* **788** 209-27
Legendre D and Maglio M 2015 Comparison between numerical models for the simulation of moving contact lines *Computers & Fluids* **113** 2-13
McHale G, Rowan S M and Newton M I 1994 Frenkel Method and the Spreading of Small Spherical Droplets *J Phys D Appl Phys* **27** 2619-23
Pahlavan A A, Cueto-Felgueroso L, McKinley G H and Juanes R 2015 Thin Films in Partial Wetting: Internal Selection of Contact-Line Dynamics *Phys. Rev. Lett.* **115**
Renardy M, Renardy Y and Li J 2001 Numerical Simulation of Moving Contact Line Problems Using a Volume-of-Fluid Method *J. Comput. Phys.* **171** 243-63
Rowan S M, Newton M I and McHale G 1995 Evaporation of Microdroplets and the Wetting of Solid Surfaces *The Journal of Physical Chemistry* **99** 13268-71

Schmuck M, Pradas M, Pavliotis G A and Kalliadasis S 2012 Upscaled phase-field models for interfacial dynamics in strongly heterogeneous domains *Proceedings of the Royal Society A: Mathematical, Physical and Engineering Science* **468** 3705-24

Schönfeld F and Hardt S 2009 Dynamic contact angles in CFD simulations *Computers & Fluids* **38** 757-64

Seaver A E and Berg J C 1994 Spreading of a Droplet on a Solid-Surface *J Appl Polym Sci* **52** 431-5

Snoeijer J H and Andreotti B 2013 Moving Contact Lines: Scales, Regimes, and Dynamical Transitions *Annual Review of Fluid Mechanics, Vol 45* **45** 269-92

Strella S 1970 Analysis of Spreading of a Viscous Drop on a Smooth Surface *J. Appl. Phys.* **41** 4242-3

Tanner L H 1979 Spreading of Silicone Oil Drops on Horizontal Surfaces *J Phys D Appl Phys* **12** 1473-84

Ververis A and Schmuck M 2017 Computational investigation of porous media phase field formulations: Microscopic, effective macroscopic, and Langevin equations *J. Comput. Phys.* **344** 485-98

Villanueva W and Amberg G 2006 Some generic capillary-driven flows *Int. J. Multiphase Flow* **32** 1072-86

Voinov O V 1976 Hydrodynamics of wetting *Fluid Dynamics* **11** 714-21

Wang X D, Peng X F, Duan Y Y and Wang B X 2007 Dynamics of spreading of liquid on solid surface *Chinese J Chem Eng* **15** 730-7

Wylock C, Pradas M, Haut B, Colinet P and Kalliadasis S 2012 Disorder-induced hysteresis and nonlocality of contact line motion in chemically heterogeneous microchannels *Phys. Fluids* **24** 032108

Yue P, Zhou C, Feng J J, Ollivier-Gooch C F and Hu H H 2006 Phase-field simulations of interfacial dynamics in viscoelastic fluids using finite elements with adaptive meshing *J. Comput. Phys.* **219** 47-67

Yue P T and Feng J J 2011 Wall energy relaxation in the Cahn-Hilliard model for moving contact lines *Phys. Fluids* **23** 012106

Yue P T, Zhou C F and Feng J J 2010 Sharp-interface limit of the Cahn-Hilliard model for moving contact lines *J. Fluid Mech.* **645** 279-94

Supplemental Material: MATLAB script

```
clear;

%%%%% Begin of Section for Parameter Input %%%%%%

% Volume of the droplet [m^3]
volume = 2.618e-10;

% Dynamic viscosity of liquid phase forming the droplet [Pa s];
mu_L = 0.03;

% Coefficient of surface tension [N/m]
sigma = 29.4e-3;

% Gas-to-liquid viscosity ratio [-]
eta = 0.01;

% Natural logarithm of ratio btw. macro- and micro-scopic length scale [-]
lamda = 10;

% Initial contact angle [-]
theta_0 = 90*pi/180;

% Equilibrium contact angle [-]
theta_e = 60*pi/180;

% Incremental step size in apparent contact angle (theta_a)
step_size = 0.0001;

% Scaling factor for static contact angle to avoid a zero denominator [-]
eps = 1.0000001;

%%%%% End of Section for Parameter Input %%%%%%

%%%%% Begin of Section for Calculation %%%%%%

% Compute volume-equivalent radius of droplet [m]
R_V = ((3*volume)/(4*pi))^(1/3);

% Compute initial spherical cap radius of droplet [m]
R_S0 = (3*volume/(pi*(2-3*cos(theta_0)+(cos(theta_0)^3))))^(1/3);

% Compute initial base radius of drop [m]
a_0 = R_S0 * sin(theta_0);

% Compute reference time scale (capillary-viscous time scale)
t_ref = ( mu_L * R_V ) / sigma;

% Constant prefactor
C = ( mu_L * lamda ) / ( sigma * (pi/(3*volume))^(1/3) );

% Function in Cox theory
```

```
one_over_f_Cox =@(x)  (eta*(x.^2-(sin(x)).^2).*(pi-x + sin(x).*cos(x)) + ((pi-
x).^2 -(sin(x)).^2).*(x-sin(x).*cos(x))./(2*sin(x).*( eta^2*(x.^2-(sin(x)).^2)
+ 2*eta*(x.*(pi-x)+(sin(x)).^2) + (pi-x).^2 -(sin(x)).^2 )) ;

% Calculate G function for equilibrium contact angle
G_e = quad(one_over_f_Cox, 0, theta_e);

% Build one-to-one maping for G and theta_a

% Counting index for building one-to-one mapping
k=1;

for theta_a= (theta_e * eps):step_size:theta_0

G(k) = quad(one_over_f_Cox, 0, theta_a);

k=k+1;

end

k=1;

for theta_a= (theta_e * eps):step_size:theta_0

F(k) =  C/((G(k)-G_e)*( (2+cos(theta_a))*(2-
3*cos(theta_a)+(cos(theta_a))^3)^(1/3)) ) ;
k=k+1;

end

m = 1;

for theta_a= (theta_e * eps):step_size:theta_0

for i= m:(k-1)
    Q(i) =  F(i)*step_size ;
end

sum = 0;

for i=m:(k-1)
    sum = sum + Q(i);
end

t(m) = sum;

m=m+1;

end

% Counting index for building one-to-one mapping relation btw. a and theta_a
k=1;
```

```
for theta_a= (theta_e*eps):step_size:theta_0
    a(k) = ((3*volume/pi)^(1/3))*sin(theta_a)/((2-
3*cos(theta_a)+(cos(theta_a)).^3).^(1/3));
    k=k+1;
end

%%%%% End of Section for Calculation %%%%%%

% Based on:
% (1) one-to-one mapping relation btw. t and theta_a,
% (2) one-to-one mapping relation btw. a  and theta_a
% we build one-to-one mapping relation btw. t and a, with the help of
% theta_a as the bridge.

% Plot the built relation as first checking:
plot(t, a);

% Write results in matrix A
% - Set matrix elements to zero:
A(k-1,4)=0;
% - Fill matrix with results:
A(:,1) = t / t_ref;
A(:,2) = t;
A(:,3) = a / a_0;
A(:,4) = a;

% Write results to file
% --- Write header
fileID = fopen('Cox_theory.txt','w');
fprintf(fileID,'%16s %16s %16s %16s \r\n','%  ln(L/L_S) [-]','theta_e
[°]','theta_0 [°]','eta [-]');
fprintf(fileID,'%c %14.6f %16.8f %16.8f %16.8f
\r\n','%',lamda,180*theta_e/pi,180*theta_0/pi,eta);
fprintf(fileID,'%16s %16s %16s %16s \r\n','%        V [m^3]','R_V [-]','R_S,0
[m]','t_ref [s]');
fprintf(fileID,'%c %14.7E %16.8E %16.8E %16.8E
\r\n','%',volume,R_V,R_S0,t_ref);
fprintf(fileID,'%16s %16s %16s %16s \r\n','tau','t','a/a_0','a');
fprintf(fileID,'%16s %16s %16s %16s \r\n','[-]','[s]','[-]','[m]');
% --- Write data
fprintf(fileID,'%16.8E %16.8E %16.8E %16.8E \r\n',0,0,1,a_0);
for i = 1:(k-1)
    fprintf(fileID,'%16.8E %16.8E %16.8E %16.8E \r\n',A(k-i,1),A(k-i,2),A(k-
i,3),A(k-i,4));
end
fclose(fileID);

% End of MATLAB script
```

Sample output of MATLAB script

```
%  ln(L/L_S) [-]      theta_e [°]      theta_0 [°]          eta [-]
%      10.000000      60.00000000      90.00000000       0.01000000
%        V [m^3]          R_V [-]        R_S,0 [m]        t_ref [s]
%  2.6180000E-10   3.96850572E-04   5.00000390E-04   4.04949564E-04
             tau                t            a/a_0                a
             [-]              [s]              [-]              [m]
  0.00000000E+00   0.00000000E+00   1.00000000E+00   5.00000390E-04
  2.21820501E-03   8.98261150E-07   1.00004934E+00   5.00025057E-04
  4.43700167E-03   1.79676189E-06   1.00009934E+00   5.00050057E-04
  6.65639025E-03   2.69550233E-06   1.00014934E+00   5.00075058E-04
  8.87637103E-03   3.59448257E-06   1.00019934E+00   5.00100058E-04
  1.10969443E-02   4.49370273E-06   1.00024934E+00   5.00125058E-04
  1.33181102E-02   5.39316292E-06   1.00029934E+00   5.00150058E-04
  1.55398692E-02   6.29286324E-06   1.00034934E+00   5.00175058E-04
  1.77622214E-02   7.19280379E-06   1.00039934E+00   5.00200058E-04
  1.99851671E-02   8.09298470E-06   1.00044934E+00   5.00225058E-04
  2.22087066E-02   8.99340606E-06   1.00049934E+00   5.00250058E-04
  2.44328402E-02   9.89406799E-06   1.00054934E+00   5.00275058E-04
  2.66575682E-02   1.07949706E-05   1.00059934E+00   5.00300058E-04
  2.88828907E-02   1.16961140E-05   1.00064934E+00   5.00325058E-04
  3.11088081E-02   1.25974983E-05   1.00069934E+00   5.00350058E-04
  3.33353207E-02   1.34991236E-05   1.00074934E+00   5.00375058E-04
  3.55624286E-02   1.44009900E-05   1.00079934E+00   5.00400058E-04
  3.77901323E-02   1.53030976E-05   1.00084934E+00   5.00425058E-04
  4.00184319E-02   1.62054465E-05   1.00089934E+00   5.00450058E-04
  4.22473277E-02   1.71080369E-05   1.00094934E+00   5.00475058E-04
  4.44768200E-02   1.80108688E-05   1.00099934E+00   5.00500058E-04
  4.67069091E-02   1.89139424E-05   1.00104934E+00   5.00525058E-04
  4.89375952E-02   1.98172578E-05   1.00109934E+00   5.00550058E-04
  5.11688785E-02   2.07208150E-05   1.00114934E+00   5.00575058E-04
  5.34007595E-02   2.16246143E-05   1.00119934E+00   5.00600059E-04
  5.56332383E-02   2.25286556E-05   1.00124934E+00   5.00625059E-04
  5.78663152E-02   2.34329391E-05   1.00129934E+00   5.00650059E-04
  6.00999906E-02   2.43374649E-05   1.00134934E+00   5.00675059E-04
  6.23342645E-02   2.52422332E-05   1.00139934E+00   5.00700059E-04
  6.45691374E-02   2.61472440E-05   1.00144934E+00   5.00725059E-04
  6.68046095E-02   2.70524975E-05   1.00149934E+00   5.00750059E-04
  6.90406811E-02   2.79579937E-05   1.00154934E+00   5.00775059E-04
  7.12773524E-02   2.88637327E-05   1.00159934E+00   5.00800059E-04
  7.35146237E-02   2.97697148E-05   1.00164934E+00   5.00825060E-04
  7.57524953E-02   3.06759399E-05   1.00169934E+00   5.00850060E-04
  7.79909675E-02   3.15824082E-05   1.00174934E+00   5.00875060E-04
  8.02300404E-02   3.24891199E-05   1.00179934E+00   5.00900060E-04
  8.24697146E-02   3.33960749E-05   1.00184934E+00   5.00925060E-04
  8.47099900E-02   3.43032735E-05   1.00189934E+00   5.00950060E-04
...
```